Am J Physiol Heart Circ Physiol 295: H1608–H1614, 2008.
First published July 11, 2008; doi:10.1152/ajpheart.01081.2007.

Strain distribution over plaques in human coronary arteries relates to shear stress

Frank J. H. Gijsen,[1] Jolanda J. Wentzel,[1,3] Attila Thury,[1] Frits Mastik,[1] Johannes A. Schaar,[1] Johan C. H. Schuurbiers,[1] Cornelis J. Slager,[1] Wim J. van der Giessen,[2,3] Pim J. de Feyter,[2] Anton F. W. van der Steen,[1,3] and Patrick W. Serruys[2]

[1]*Department of Biomedical Engineering and* [2]*Interventional Cardiology, Thoraxcenter, Erasmus Medical Center, Rotterdam; and* [3]*Interuniversity Cardiology Institute of the Netherlands, Utrecht, The Netherlands*

Submitted 18 September 2007; accepted in final form 8 July 2008

Gijsen FJ, Wentzel JJ, Thury A, Mastik F, Schaar JA, Schuurbiers JC, Slager CJ, van der Giessen WJ, de Feyter PJ, van der Steen AF, Serruys PW. Strain distribution over plaques in human coronary arteries relates to shear stress. *Am J Physiol Heart Circ Physiol* 295: H1608–H1614, 2008. First published July 11, 2008; doi:10.1152/ajpheart.01081.2007.—Once plaques intrude into the lumen, the shear stress they are exposed to alters with hitherto unknown consequences for plaque composition. We investigated the relationship between shear stress and strain, a marker for plaque composition, in human coronary arteries. We imaged 31 plaques in coronary arteries with angiography and intravascular ultrasound. Computational fluid dynamics was used to obtain shear stress. Palpography was applied to measure strain. Each plaque was divided into four regions: upstream, throat, shoulder, and downstream. Average shear stress and strain were determined in each region. Shear stress in the upstream, shoulder, throat, and downstream region was 2.55 ± 0.89, 2.07 ± 0.98, 2.32 ± 1.11, and 0.67 ± 0.35 Pa, respectively. Shear stress in the downstream region was significantly lower. Strain in the downstream region was also significantly lower than the values in the other regions (0.23 ± 0.08% vs. 0.48 ± 0.15%, 0.43 ± 0.17%, and 0.47 ± 0.12%, for the upstream, shoulder, and throat regions, respectively). Pooling all regions, dividing shear stress per plaque into tertiles, and computing average strain showed a positive correlation; for low, medium, and high shear stress, strain was 0.23 ± 0.10%, 0.40 ± 0.15%, and 0.60 ± 0.18%, respectively. Low strain colocalizes with low shear stress downstream of plaques. Higher strain can be found in all other plaque regions, with the highest strain found in regions exposed to the highest shear stresses. This indicates that high shear stress might destabilize plaques, which could lead to plaque rupture.

atherosclerosis; coronary artery disease; intravascular ultrasound; palpography

THE AVERAGE blood flow-induced shear stress (SS) in healthy arteries is ~1 Pa (20). Although it is several orders of magnitude smaller than blood pressure, SS has a strong impact on endothelial function. It is well accepted that low and/or oscillating SS causes endothelial dysfunction and is one of the key players in localizing early atherosclerosis (20, 33, 40, 43). On the other hand, normal and high SS is atheroprotective and is involved in compensatory remodeling (11, 33).

At a certain point, compensatory remodeling fails, and the plaque will intrude into the lumen. The transition from compensatory remodeling to plaque intrusion into the lumen is poorly understood (33), but intraplaque hemorrhage might play a role (1). Even a slight intrusion into the lumen will result in a change of the SS pattern over the plaque. Some plaque regions will be exposed to higher SS levels, whereas in other regions (notably downstream of a lumen-intruding plaque), SS will decrease. The possible effects of these changes in SS over lumen-intruding plaques was reviewed by Slager et al. (34). They identified various pathways along which increased SS levels could influence plaque composition in such a way that it enhances plaque vulnerability. These pathways include nitric oxide-mediated smooth muscle cell (SMC) apoptosis and plasmin-induced metalloproteinase activity. Plaque regions exposed to decreased SS levels remain proatherogenetic. Apart from a continued influx from lipids and proinflammatory cells, there are several pathways that could induce SMC proliferation and matrix synthesis. These pathways include the effect of platelet-derived growth factors and endothelin-1, both potent vascular smooth muscle cell mitogens (for a review, see Ref. 2). An observational study by Dirksen et al. (8) showed indeed that the downstream region of lumen-intruding plaques in the carotid bifurcation contained more SMCs compared with those of the upstream region.

The mechanism described above might be especially relevant, but not limited to, vulnerable plaques. The mechanical trigger for the rupture of a vulnerable plaque, the main cause of unstable angina and acute myocardial infarction (30), is most likely a blood pressure peak (27). Blood pressure can induce high tensile stresses in the cap of a vulnerable plaque (17), especially in the presence of microcalcifications (42). If these tensile stresses exceed the local fracture stress of a cap, rupture will occur. The local fracture stress of a cap is determined by several factors, the most important being local cap thickness and composition (26). The cap is a structure in a dynamic state, and its composition is determined by many factors including collagen synthesis by SMCs and collagen breakdown by metalloproteinases (16). Blood flow-induced SS might be one of the factors that influences the processes that govern cap morphology and composition (8, 10, 12, 18, 36).

The aim of this study is to investigate the relationship between SS and plaque composition in human coronary arteries in vivo. For this purpose, we use two intravascular ultrasound (IVUS)-based imaging techniques. The first concerns biplane angiography and intravascular ultrasound (ANGUS) and provides detailed three-dimensional geometrical information, which is used to determine the wall thickness and the SS

Address for reprint requests and other correspondence: F. Gijsen, Dept. of Biomedical Engineering, Ee2322, Erasmus Medical Center, PO Box 2040, 3000 CA Rotterdam, The Netherlands (e-mail: f.gijsen@erasmusmc.nl).

The costs of publication of this article were defrayed in part by the payment of page charges. The article must therefore be hereby marked "*advertisement*" in accordance with 18 U.S.C. Section 1734 solely to indicate this fact.

distribution. The second imaging modality is palpography (9), which measures local radial strain (STR) in the vessel wall, induced by the blood pressure. In general, plaque regions with lower wall stiffness will reveal higher STR values, and where wall stiffness is higher, the STR values will be lower. In vitro studies have shown that STR measurements can be used to discriminate between fibrous, fatty-fibrous, and fatty arterial tissue (5). It was also shown in vivo that plaques containing calcium showed lower STR values than those of noncalcified plaques (4) and that fatty plaques showed higher STR values (6). In diseased human coronary arteries, measured STR values showed a strong positive correlation with macrophage concentration and a negative correlation with smooth muscle cell content (29). These in vivo experiments demonstrate that STR values over a plaque, measured with palpography, can be regarded as a surrogate marker of local plaque composition (32). The two imaging modalities are combined to study the distribution of STR over plaques and to relate this marker of plaque composition to local SS values.

MATERIALS AND METHODS

Patients. We investigated 13 native coronary arteries in 12 patients who participated in the Integrated Biomarker and Imaging Study (IBIS), a single center, prospective, nonrandomized observational study (39). Patients with stable angina, silent ischemia, or an acute coronary syndrome referred for percutaneous coronary intervention were eligible. The aim of the IBIS study was to assess nonflow-limiting coronary lesions using invasive and noninvasive imaging techniques in conjunction with biomarkers in a coronary artery, other than the artery that was the target for intervention.

The Institutional Medical Ethical Committee approved the study protocol, and all patients gave written informed consent to participate in this study.

Three-dimensional coronary artery imaging. The ANGUS procedure combines biplane angiography with IVUS to obtain the three-dimensional geometry of the coronary arteries. Briefly, a sheath-based IVUS catheter with a rotating element (UltraCross 2.9 or CVIS Atlantis; Boston Scientific) was positioned distal in the artery and imaged using a biplane angiographic system (Bicor; Siemens). IVUS images were acquired during an ECG-gated motorized pullback (EchoScan; TomTec) with a step size of 0.5 mm. Contours of the lumen and the media-bounded area (the latter were based on the external elastic lamina) were drawn in the IVUS images and subsequently stacked on the three-dimensional reconstruction of the path of the catheter that was derived from the initial biplane angiographic recordings. The three-dimensional lumen reconstruction served as input for the computation of the SS distribution, and the distance between the lumen and media-bounded area was used to derive the wall thickness distribution. Details regarding the ANGUS procedure are described elsewhere (35).

Shear stress. The SS distribution was obtained by solving the Navier-Stokes equations on a finite element mesh that represented the reconstructed three-dimensional lumen of the coronary artery (15). The boundary conditions for the finite element analysis consisted of patient-specific data. Flow through the artery was derived from average velocity measured by quantitative IVUS blood flow (20 MHz Avanar; Volcano Therapeutics) (19). The measured flow was used to generate a parabolic velocity profile at the inlet of the artery. No-slip boundary conditions were used at the lumen wall, and stress-free outflow was prescribed. We applied a shear thinning power-law model for blood, using the measured viscosity, hematocrit, and fibrinogen (25). The Navier-Stokes equations were solved with a validated finite element code (SEPRAN, SEPRA BV). For more details on the computational methods, see supplemental data (supplemental data can be found with the online version of this article).

Strain. IVUS palpography measures the STR in the direction of the ultrasound beam in the inner layer of the vessel wall. The STR distribution is inferred from data acquired during a continuous (0.5 or 1 mm/s) IVUS pullback (Trackback II; Volcano Therapeutics) with a commercially available catheter (20 MHz Avanar; Volcano Therapeutics). IVUS palpography measures the radial STR in the inner layer of the wall of a coronary artery that is deformed by variations in the arterial pressure pulse (9). The STR values are determined by applying cross-correlation techniques on the reflected radio frequency ultrasound signals from two different time points of the arterial pressure pulse (7). The STR values were normalized by average pressure drop between the two time points. The STR values from one heart cycle were averaged to determine the compounded STR distribution, which we used in the current analysis (9). It was shown that the STR distribution, as can be measured with palpography, is a surrogate marker for plaque composition (29).

Image registration. Since the SS imaging and the STR imaging use data from different IVUS catheters, the two data sets were registered. This was achieved by carefully matching the underlying IVUS images of the two data sets. Anatomical landmarks, including side branches and calcified spots, were identified in both image stacks. Based on these landmarks, two second-order polynomial fits were derived to register the two image stacks: one for matching the IVUS images in the axial direction and one for the rotation of the IVUS images. We used, on average, 5.4 $\pm$ 1.6 landmarks to match the two data sets. Only the region in between the most distal and most proximal landmark observed in both data sets was used for further analysis. We excluded regions containing IVUS artifacts that could be indicative of a nonuniform pullback speed.

Data analysis and statistics. Segments between side branches were analyzed. Plaques were identified based on wall thickness data. Plaques were considered to be present at those locations where wall thickness was larger than 20% of the local lumen diameter (Fig. 1) (44). Plaques were selected, and plaque burden [plaque burden = (vessel area $-$ lumen area)/ vessel area $\times$ 100%] was determined at minimal lumen diameter for each plaque. At that same location, we also determined area stenosis [area stenosis = (lumen area at the reference cross section $-$ lumen area)/lumen area at the reference cross section $\times$ 100%] and remodeling [remodeling = (vessel area $-$ vessel at the reference cross section)/vessel area at the reference cross section $\times$ 100%]. The reference cross section was defined as the cross section with a maximum lumen area in the segment that contained the plaque.

Subsequently, the plaques were divided into regions: upstream, throat, downstream, and lateral shoulders (Fig. 1). These regions covered the complete plaque. The average SS and STR values were determined in each region, and these average values form the basis for the analyses in this study.

One-way ANOVA with post hoc testing was applied to compare mean values. Regression analyses were applied to study the relationship between SS and STR per plaque. *P* values smaller than 0.05 were considered to be statistically significant. All statistical analyses were carried out with SPSS (version 11.3; SPSS).

RESULTS

Plaque characteristics. We analyzed 13 coronary arteries in 12 patients. The study vessel was the right coronary in 7 of 13 arteries, the left anterior descending in 4 of 13 arteries, and the left circumflex in 2 of 13 arteries. The demographic and clinical patient characteristics are given in Table 1. The three-dimensional geometry of all arteries was successfully reconstructed with the ANGUS procedure. The registration of the two IVUS data sets failed in one artery; the region in which the two data sets overlapped contained only a single identifiable

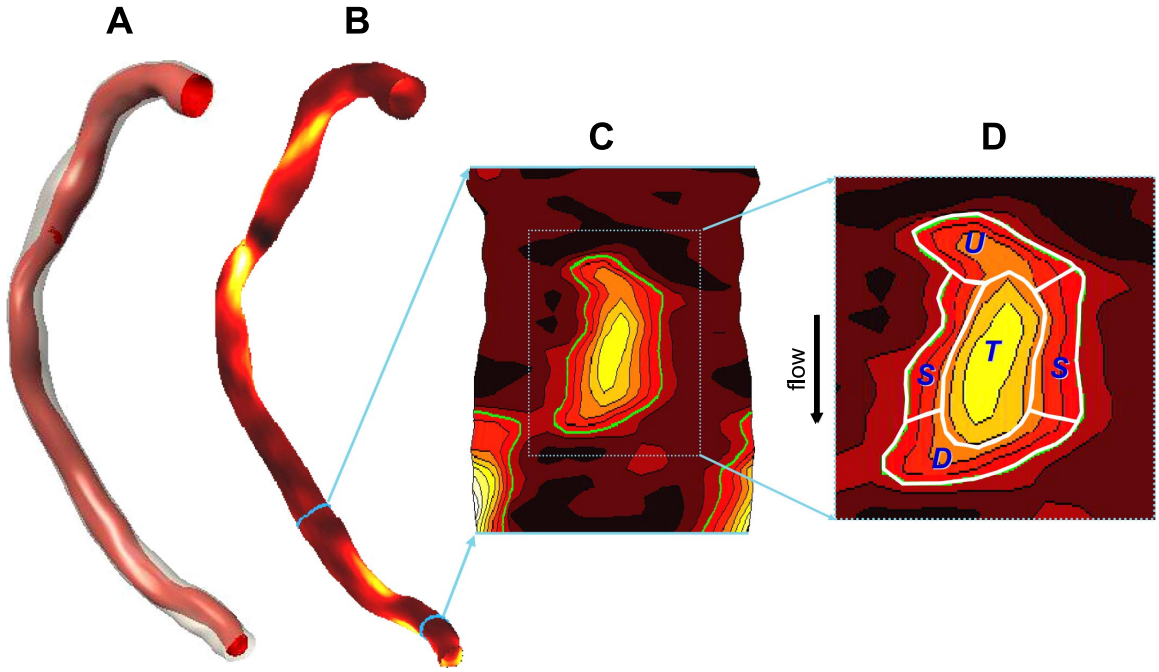

Fig. 1. The results of the 3-dimensional reconstruction of a right coronary artery are given in *A*. The lumen is in red, and the media-bounded area is represented in gray. The normalized wall thickness is projected on the lumen in *B* (red/brown is low, and yellow/white is high). A 2-dimensional anatomical representation of a part of the lumen is given in *C*, where the normalized wall thickness (WT_{norm}) contour that defines a plaque ($WT_{norm} = 0.2$) is demarcated by the green line. The specific plaque regions [upstream (U), throat (T), lateral shoulder (S), and downstream (D)] are given in *D*.

anatomical landmark. The remaining 12 arteries rendered 25 segments between side branches, four of which were free of any disease. The remaining 21 matched segments had an average length of 21 ± 10 mm with an average diameter of 3.1 ± 0.6 mm. The segments were exposed to an average SS of 1.28 ± 0.16 Pa and an average STR of 0.33 ± 0.15% at a mean pressure drop of 2.5 ± 1.1 mmHg. The average wall thickness was 0.47 ± 0.09 mm. In the matched segments, 31 plaques were present with an average plaque burden of 50 ± 12%. The average area stenosis of the plaques was 36 ± 22%, and positive remodeling was observed (8 ± 9%). Out of 31 plaques, five showed calcifications on IVUS. In the axial direction, the plaques were 6.3 ± 3.1 mm long and in the circumferential direction they extended over an angle of 192 ± 68°.

Table 1. *Patient characteristics*

Number of patients	12
Number of vessels	13
Vessel	
Right coronary artery	7
Left anterior descending	4
Left circumflex	2
Sex	
Male	11
Female	1
Age	59±13
Hypercholesteremia	12
Hypertension	6
Diabetes	1
Systolic blood pressure, mmHg	142±19
Diastolic blood pressure, mmHg	80±7
Average flow rate, ml/min	105±63
Clinical presentation	
Unstable angina	3
Stable angina	8
Silent ischemia	1

Values are means ± SE.

SS versus location. The average SS over the plaques was 1.82 ± 1.14 Pa, being 42% higher than the average SS in the complete segment, which contains the plaque. For all plaques, the respective average SS values in the upstream, shoulder, throat, and downstream region were 2.55 ± 0.89, 2.07 ± 0.98, 2.32 ± 1.11, and 0.67 ± 0.35 Pa, respectively (Fig. 2, *top*). We did not observe negative SS values in the downstream region, which indicates that no flow reversal is present. The average SS in the downstream region was significantly lower than in all the other regions ($P < 0.05$). Upstream, shoulders, and throat were exposed to similar SS levels.

STR versus location. The average STR over the plaque was 0.40 ± 0.13%, which is 15% higher than the average STR in the complete segment in which the plaque is located. The pattern of the STR distribution over the plaque was similar to the pattern observed for the SS: comparable values at the upstream, shoulder, and throat region of the plaque and lower STR values downstream of the plaque. The average STR values for all the plaques in the upstream, shoulder, throat, and downstream region were 0.48 ± 0.15%, 0.47 ± 0.12%, 0.43 ± 0.17%, and 0.23 ± 0.08% (Fig. 2, *bottom*). Downstream, the STR was significantly lower than at all the other locations ($P < 0.05$).

SS versus STR. We investigated the relationship between average SS and average STR over each plaque using regression analysis. An example is shown in Fig. 3; the regression line shows a positive slope: regions exposed to low SS exhibit low STR and the STR increases with increasing SS. From the 31 plaques, 29 showed a positive relationship. The average slope for all the plaques was 0.28 ± 0.15% Pa ($P <$

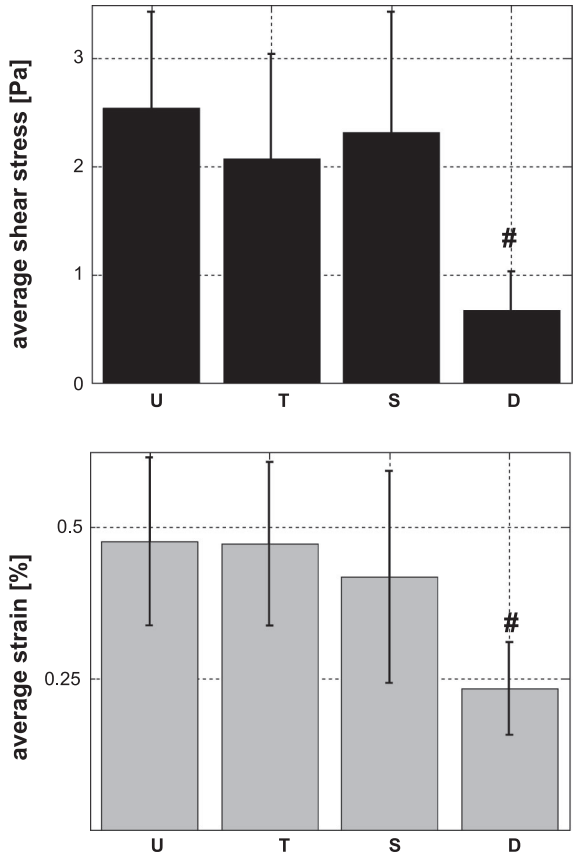

Fig. 2. Average shear stress (*top*) and average strain (*bottom*) for each plaque region (U, T, D, and S). #Significant difference at a $P < 0.05$ level.

0.001), implying that the STR increases 0.28% with each Pa the SS increases.

To be able to compare the data from all the plaques, we divided the SS values into tertiles for each plaque. The SS in each plaque region was labeled as low, medium, or high, depending on its value. The data of all the plaques were pooled, and the average STR for each SS tertile was computed. The average STR in the lowest SS tertile was 0.23 ± 0.010%, in the medium SS tertile the average STR was 0.40 ± 0.15%, and in the highest SS tertile the average STR was 0.60 ± 0.18% (Fig. 4). All values were significantly different from each other at a $P < 0.01$ level.

DISCUSSION

This study is the first to provide combined data on the distribution of SS and STR over plaques in human coronary arteries in vivo. The data enabled us to study the relationship between SS and STR, a surrogate marker for plaque composition. We found that low STR values colocalize with low SS values downstream of a plaque. Higher STR values can be found in all the other plaque regions, with the highest STR values found in regions exposed to the highest SS.

SS versus location. The SS distribution in often idealized geometrical models of human coronary arteries was the subject of numerous investigations (14, 15, 24, 36, 44), and in these studies it was shown that the geometry of coronary arteries is the main determinant of the observed SS distribution. Generally, downstream of a plaque, low SS can be expected, which was confirmed in the current investigation. The results of this study show that complex three-dimensional shape of the coronary artery does not permit the prediction of the SS in the other regions; the SS in a specific plaque region is influenced by the patient-specific proximal geometry of the artery.

STR versus location. The wall stiffness of a plaque region is mainly determined by its composition. The STR distribution, as was measured by palpography, can therefore be regarded as a surrogate marker for plaque composition. Postmortem experiments have shown that plaque regions with a high concentration of SMCs correlate with low STR values and can therefore be considered to be stiffer. Plaque regions with large amount of macrophages show high STR values and thus have a lower wall stiffness (29). The measured STR distribution over coronary plaques from this study reveal that low STR values are present in the downstream regions, indicating that the vessel wall is stiffer there than it is at the other plaque locations. The observed increased SMC concentration in the downstream region of carotid plaques (8) as well as earlier proposed mechanobiological mechanisms (34) agree well with this observation. The results of the current study also revealed that, compared with the downstream regions, the upstream regions of the plaques showed higher STR values. This observation agrees with the observed higher concentration of macrophages in the upstream region of carotid plaques (8). The STR values in the upstream, throat, and shoulder regions showed a heterogeneous distribution, indicating that, apart from downstream, location alone does not govern the composition of the plaque. Since one can expect an inverse relationship between wall thickness and STR, this could be a confounding factor in the current study. However, since STR is larger in the throat region (the region where wall thickness is largest) than in the downstream region (where wall thickness is lower), the composition of the plaque seems to govern the measured STR distribution.

SS versus STR. SS itself does not induce deformation of the plaque; wall stresses, induced by blood pressure, are ~100,000 times higher than SS and are most likely the mechanical trigger of plaque rupture (27). Although the direct mechanical impact of SS is limited, SS has an important effect on endothelial function (38), and results from basic research and clinical observations suggest a biological effect of SS on plaque composition (21). It was hypothesized (34) that plaque regions exposed to high SS might be weakened due to matrix breakdown by plasmin-induced metalloproteinases and the regression of the SMC. One can speculate that, when applying these findings to vulnerable plaques, cap thickness in regions exposed to high SS might be reduced. Combined with the effect of microcalcifications (41, 42), this might enhance plaque vulnerability. In plaque regions exposed to low SS, atherosclerosis might progress due to endothelial dysfunction with the accompanying SMC proliferation. The relationship between SS and STR and their spatial distribution over the plaques we found in this study agree with this hypothesis: the downstream region of the plaque, exposed to low SS, is stiffer, pointing at an increased SMC concentration. In the other regions, high SS coincides with high STR, indicating that weaker material is present at those locations.

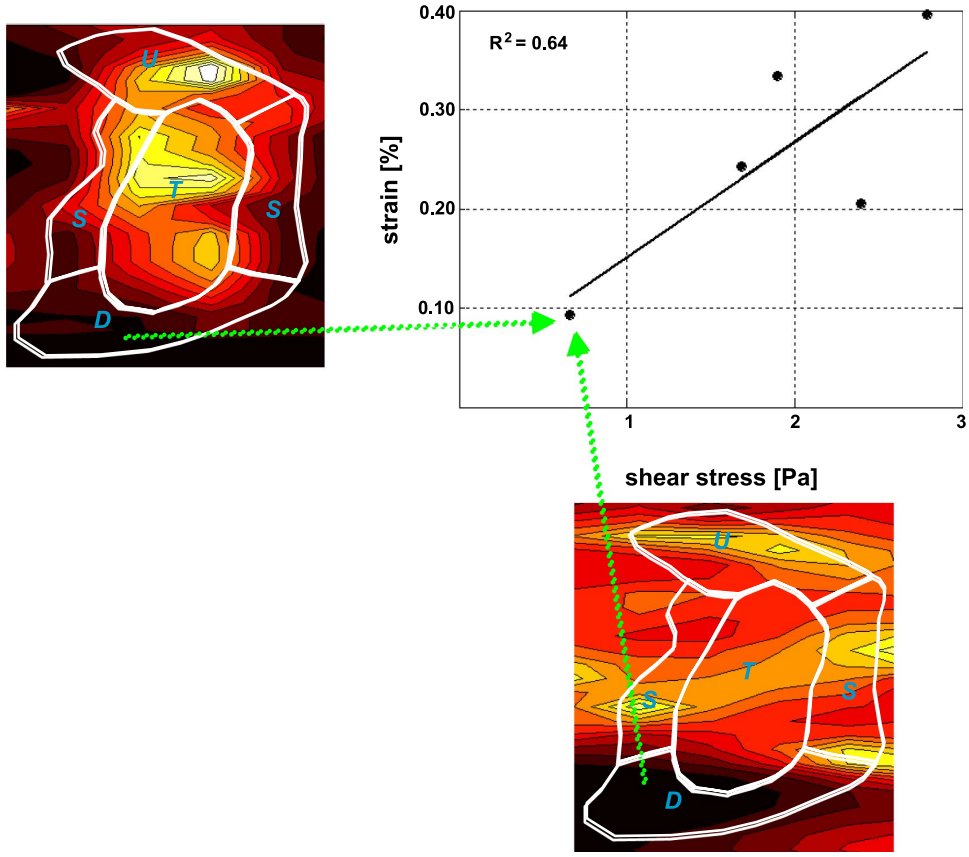

Fig. 3. Average shear stress vs. the average strain in the regions covering a plaque. The downstream (D) region is exposed to low shear stress, and low strain values were measured at that location (green arrow). In the other regions, the measured strain increased with the shear stress the regions were exposed to.

Limitations

This study has certain limitations. First, the patient population and the number of plaques investigated are small. We determined the peak STR before pressure normalization for each plaque to be able to categorize them according to the validated Rotterdam classification (ROC) classification (39). The ROC I classification was used for plaques with a peak STR between 0% and 0.6%, ROC II for a peak STR between 0.6% and 0.9%, ROC III for a peak STR between 0.9% and 1.2%, and ROC IV for a peak STR over 1.2%. Using these values to separate the plaques, we found that 10 plaques were ROC I, six plaques were ROC II, 10 were ROC III, and five plaques were ROC IV. The incidence of ROC values of the plaques in this study is in good agreement with previously reported data (31), indicating that our patient population spans a wide range of the overall population of the IBIS trial. Increasing the number of plaques combined with data over time would be especially relevant if we would like to further investigate the various hypothesis on the possible influence of SS on the composition of vulnerable plaques (3, 34). Second, we have to consider the accuracy with which the image registration was performed. Based on the results of the polynomial fitting procedure, we estimate the axial mapping to be accurate within 0.5 mm and the circumferential mapping within 5°. With the average size of the plaques in this study (6.3 mm and 192°) taken into account, it is unlikely that mismatch in image registration confounds the observed relationship between SS and STR. Although we do not expect mismatch in image registration to be a major source of error, studies like these could benefit from simultaneous SS and plaque composition imaging. This can be achieved by the application of the sheath-based IVUS catheter with a rotating element, which can be used for both the ANGUS procedure and IVUS virtual histology (28). Finally, palpography measures radial STR and cannot visualize plaque composition directly, and it suffers from limited resolution. Several imaging modalities emerged that can provide information on plaque composition based on spectroscopy (22, 23) but more studies need to be carried out to validate them. Once the imaging techniques for plaque composition are established, we can combine this information with palpography to extend the

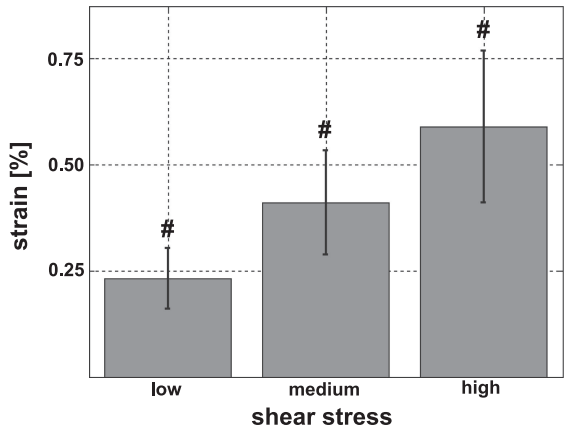

Fig. 4. The average strain at the 3 shear stress levels. #Significant different average strain values at a $P < 0.01$ level.

computational framework to include fluid-solid interaction, like some of the studies concerning plaque deformation in carotid arteries (37). Such coupled computations will contribute to a more complete understanding of plaque mechanics. The combination of palpography with high-resolution optical coherence tomography (13) seems to be a promising approach to identify plaques with thin caps and high STR spots, a possible fingerprint of plaque vulnerability.

Conclusions

The findings from this study demonstrate for the first time a relationship between blood flow-induced SS and STR in human coronary arteries in vivo. Plaque regions downstream of plaques are exposed to low SS, and the low STR values found indicate that the plaque is stiffer there. Plaque regions, exposed to high SS, show high STR values, indicating weaker underlying wall material, and these regions might therefore be more prone to rupture. It can be speculated that the regions of a cap of a vulnerable plaque, exposed to high SS, will continue to weaken over time, eventually leading to the rupture of the cap.

REFERENCES

1. **Burke AP, Kolodgie FD, Farb A, Weber D, Virmani R.** Morphological predictors of arterial remodeling in coronary atherosclerosis. *Circulation* 105: 297–303, 2002.
2. **Chatzizisis YS, Coskun AU, Jonas M, Edelman ER, Feldman CL, Stone PH.** Role of endothelial shear stress in the natural history of coronary atherosclerosis and vascular remodeling: molecular, cellular, and vascular behavior. *J Am Coll Cardiol* 49: 2379–2393, 2007.
3. **Chatzizisis YS, Jonas M, Coskun AU, Beigel R, Stone BV, Maynard C, Gerrity RG, Daley W, Rogers C, Edelman ER, Feldman CL, Stone PH.** Prediction of the localization of high-risk coronary atherosclerotic plaques on the basis of low endothelial shear stress: an intravascular ultrasound and histopathology natural history study. *Circulation* 117: 993–1002, 2008.
4. **de Korte CL, Carlier SG, Mastik F, Doyley MM, van der Steen AF, Serruys PW, Bom N.** Morphological and mechanical information of coronary arteries obtained with intravascular elastography; feasibility study in vivo. *Eur Heart J* 23: 405–413, 2002.
5. **de Korte CL, Pasterkamp G, van der Steen AF, Woutman HA, Bom N.** Characterization of plaque components with intravascular ultrasound elastography in human femoral and coronary arteries in vitro. *Circulation* 102: 617–623, 2000.
6. **de Korte CL, Sierevogel MJ, Mastik F, Strijder C, Schaar JA, Velema E, Pasterkamp G, Serruys PW, van der Steen AF.** Identification of atherosclerotic plaque components with intravascular ultrasound elastography in vivo: a Yucatan pig study. *Circulation* 105: 1627–1630, 2002.
7. **de Korte CL, van der Steen AF, Cespedes EI, Pasterkamp G.** Intravascular ultrasound elastography in human arteries: initial experience in vitro. *Ultrasound Med Biol* 24: 401–408, 1998.
8. **Dirksen MT, van der Wal AC, van den Berg FM, van der Loos CM, Becker AE.** Distribution of inflammatory cells in atherosclerotic plaques relates to the direction of flow. *Circulation* 98: 2000–2003, 1998.
9. **Doyley MM, Mastik F, de Korte CL, Carlier SG, Cespedes EI, Serruys PW, Bom N, van der Steen AF.** Advancing intravascular ultrasonic palpation toward clinical applications. *Ultrasound Med Biol* 27: 1471–1480, 2001.
10. **Fujii K, Kobayashi Y, Mintz GS, Takebayashi H, Dangas G, Moussa I, Mehran R, Lansky AJ, Kreps E, Collins M, Colombo A, Stone GW, Leon MB, Moses JW.** Intravascular ultrasound assessment of ulcerated ruptured plaques: a comparison of culprit and nonculprit lesions of patients with acute coronary syndromes and lesions in patients without acute coronary syndromes. *Circulation* 108: 2473–2478, 2003.
11. **Glagov S, Weisenberg E, Zarins CK, Stankunavicius R, Kolettis GJ.** Compensatory enlargement of human atherosclerotic coronary arteries. *N Engl J Med* 316: 1371–1375, 1987.
12. **Groen HC, Gijsen FJ, van der Lugt A, Ferguson MS, Hatsukami TS, van der Steen AF, Yuan C, Wentzel JJ.** Plaque rupture in the carotid artery is localized at the high shear stress region: a case report. *Stroke* 38: 2379–2381, 2007.
13. **Jang IK, Tearney GJ, MacNeill B, Takano M, Moselewski F, Iftima N, Shishkov M, Houser S, Aretz HT, Halpern EF, Bouma BE.** In vivo characterization of coronary atherosclerotic plaque by use of optical coherence tomography. *Circulation* 111: 1551–1555, 2005.
14. **Joshi AK, Leask RL, Myers JG, Ojha M, Butany J, Ethier CR.** Intimal thickness is not associated with wall shear stress patterns in the human right coronary artery. *Arterioscler Thromb Vasc Biol* 24: 2408–2413, 2004.
15. **Krams R, Wentzel J, Oomen J, Vinke R, Schuurbiers J, de Feyter P, Serruys P, Slager C.** Evaluation of endothelial shear stress and 3D geometry as factors determining the development of atherosclerosis and remodeling in human coronary arteries in vivo. Combining 3D reconstruction from angiography and IVUS (ANGUS) with computational fluid dynamics. *Arterioscler Thromb Vasc Biol* 17: 2061–2065, 1997.
16. **Lee RT, Libby P.** The unstable atheroma. *Arterioscler Thromb Vasc Biol* 17: 1859–1867, 1997.
17. **Loree HM, Kamm RD, Stringfellow RG, Lee RT.** Effects of fibrous cap thickness on peak circumferential stress in model atherosclerotic vessels. *Circ Res* 71: 850–858, 1992.
18. **Lovett JK, Rothwell PM.** Site of carotid plaque ulceration in relation to direction of blood flow: an angiographic and pathological study. *Cerebrovasc Dis* 16: 369–375, 2003.
19. **Lupotti FA, Mastik F, Carlier SG, de Korte CL, van der Giessen WJ, Serruys PW, van der Steen AFW.** Quantitative IVUS blood flow: validation in vitro, in animals and in patients. *Ultrasound Med Biol* 29: 507–515, 2003.
20. **Malek AM, Alper SL, Izumo S.** Hemodynamic shear stress and its role in atherosclerosis. *JAMA* 282: 2035–2042, 1999.
21. **Mattsson EJ, Kohler TR, Vergel SM, Clowes AW.** Increased blood flow induces regression of intimal hyperplasia. *Arterioscler Thromb Vasc Biol* 17: 2245–2249, 1997.
22. **Moreno PR, Purushothaman KR, Fuster V, Echeverri D, Truszczynska H, Sharma SK, Badimon JJ, O'Connor WN.** Plaque neovascularization is increased in ruptured atherosclerotic lesions of human aorta: implications for plaque vulnerability. *Circulation* 110: 2032–2038, 2004.
23. **Nair A, Kuban BD, Tuzcu EM, Schoenhagen P, Nissen SE, Vince DG.** Coronary plaque classification with intravascular ultrasound radiofrequency data analysis. *Circulation* 106: 2200–2206, 2002.
24. **Perktold K, Hofer M, Rappitsch G, Loew M, Kuban B, Friedman M.** Validated computation of physiologic flow in a realistic coronary artery branch. *J Biomech* 31: 217–228, 1998.
25. **Pop GAM, Hop WJ, van der Jagt M, Quak J, Dekkers D, Chang Z, Gijsen FJ, Duncker DJ, Slager CJ.** Blood electrical impedance closely matches whole blood viscosity as parameter of hemorheology and inflammation. *Appl Rheol* 13: 305–312, 2003.
26. **Richardson PD.** Biomechanics of plaque rupture: progress, problems, and new frontiers. *Ann Biomed Eng* 30: 524–536, 2002.
27. **Richardson PD, Davies MJ, Born GV.** Influence of plaque configuration and stress distribution on fissuring of coronary atherosclerotic plaques. *Lancet* 2: 941–944, 1989.
28. **Rodriguez-Granillo GA, Garcia-Garcia HM, Mc Fadden EP, Valgimigli M, Aoki J, de Feyter P, Serruys PW.** In vivo intravascular ultrasound-derived thin-cap fibroatheroma detection using ultrasound radiofrequency data analysis. *J Am Coll Cardiol* 46: 2038–2042, 2005.
29. **Schaar JA, De Korte CL, Mastik F, Strijder C, Pasterkamp G, Boersma E, Serruys PW, Van Der Steen AF.** Characterizing vulnerable plaque features with intravascular elastography. *Circulation* 108: 2636–2641, 2003.
30. **Schaar JA, Muller JE, Falk E, Virmani R, Fuster V, Serruys PW, Colombo A, Stefanadis C, Ward Casscells S, Moreno PR, Maseri A, Van Der Steen AF.** Terminology for high-risk and vulnerable coronary artery plaques. *Eur Heart J* 25: 1077–1082, 2004.
31. **Schaar JA, Regar E, Mastik F, McFadden EP, Saia F, Disco C, de Korte CL, de Feyter PJ, van der Steen AF, Serruys PW.** Incidence of high-strain patterns in human coronary arteries: assessment with three-dimensional intravascular palpography and correlation with clinical presentation. *Circulation* 109: 2716–2719, 2004.
32. **Schaar JA, van der Steen AF, Mastik F, Baldewsing RA, Serruys PW.** Intravascular palpography for vulnerable plaque assessment. *J Am Coll Cardiol* 47: C86–C91, 2006.
33. **Slager CJ, Wentzel JJ, Gijsen FJ, Schuurbiers JC, van der Wal AC, van der Steen AF, Serruys PW.** The role of shear stress in the generation

of rupture-prone vulnerable plaques. *Nat Clin Pract Cardiovasc Med* 2: 401–407, 2005.

34. **Slager CJ, Wentzel JJ, Gijsen FJ, Thury A, van der Wal AC, Schaar JA, Serruys PW.** The role of shear stress in the destabilization of vulnerable plaques and related therapeutic implications. *Nat Clin Pract Cardiovasc Med* 2: 456–464, 2005.
35. **Slager CJ, Wentzel JJ, Schuurbiers JC, Oomen JA, Kloet J, Krams R, von Birgelen C, van der Giessen WJ, Serruys PW, de Feyter PJ.** True 3-dimensional reconstruction of coronary arteries in patients by fusion of angiography and IVUS (ANGUS) and its quantitative validation. *Circulation* 102: 511–516, 2000.
36. **Stone PH, Coskun AU, Kinlay S, Clark ME, Sonka M, Wahle A, Ilegbusi OJ, Yeghiazarians Y, Popma JJ, Orav J, Kuntz RE, Feldman CL.** Effect of endothelial shear stress on the progression of coronary artery disease, vascular remodeling, and in-stent restenosis in humans: in vivo 6-month follow-up study. *Circulation* 108: 438–444, 2003.
37. **Tang D, Yang C, Zheng J, Woodard PK, Saffitz JE, Sicard GA, Pilgram TK, Yuan C.** Quantifying effects of plaque structure and material properties on stress distributions in human atherosclerotic plaques using 3D FSI models. *J Biomech Eng* 127: 1185–1194, 2005.
38. **Tricot O, Mallat Z, Heymes C, Belmin J, Leseche G, Tedgui A.** Relation between endothelial cell apoptosis and blood flow direction in human atherosclerotic plaques. *Circulation* 101: 2450–2453, 2000.
39. **Van Mieghem CA, Bruining N, Schaar JA, McFadden E, Mollet N, Cademartiri F, Mastik F, Ligthart JM, Granillo GA, Valgimigli M, Sianos G, van der Giessen WJ, Backx B, Morel MA, Van Es GA, Sawyer JD, Kaplow J, Zalewski A, van der Steen AF, de Feyter P, Serruys PW.** Rationale and methods of the integrated biomarker and imaging study (IBIS): combining invasive and non-invasive imaging with biomarkers to detect subclinical atherosclerosis and assess coronary lesion biology. *Int J Card Imaging* 21: 425–441, 2005.
40. **VanderLaan PA, Reardon CA, Getz GS.** Site specificity of atherosclerosis: site-selective responses to atherosclerotic modulators. *Arterioscler Thromb Vasc Biol* 24: 12–22, 2004.
41. **Vengrenyuk Y, Cardoso L, Weinbaum S.** Micro-CT based analysis of a new paradigm for vulnerable plaque rupture: cellular microcalcifications in fibrous caps. *Mol Cell Biomech* 5: 37–47, 2008.
42. **Vengrenyuk Y, Carlier S, Xanthos S, Cardoso L, Ganatos P, Virmani R, Einav S, Gilchrist L, Weinbaum S.** A hypothesis for vulnerable plaque rupture due to stress-induced debonding around cellular microcalcifications in thin fibrous caps. *Proc Natl Acad Sci USA* 103: 14678–14683, 2006.
43. **Weinbaum S, Tzeghai G, Ganatos P, Pfeffer R, Chien S.** Effect of cell turnover and leaky junctions on arterial macromolecular transport. *Am J Physiol Heart Circ Physiol* 248: H945–H960, 1985.
44. **Wentzel JJ, Janssen E, Vos J, Schuurbiers JC, Krams R, Serruys PW, de Feyter PJ, Slager CJ.** Extension of increased atherosclerotic wall thickness into high shear stress regions is associated with loss of compensatory remodeling. *Circulation* 108: 17–23, 2003.